High-Resolution DNA Binding Kinetics Measurements with Double Gate FD-SOI Transistors

Seulki Cho[1], Alexander Zaslavsky[1,2], Curt A. Richter[1], Jacob M. Majikes[1], J. Alexander Liddle[1], François Andrieu[3], Sylvain Barraud[3], and Arvind Balijepalli[1]
[1]National Institute of Standards and Technology, Gaithersburg, MD, USA, email: arvind.balijepalli@nist.gov
[2]Brown University, Providence RI, USA, [3]CEA-LETI, Univ. Grenoble Alpes, 38000 Grenoble, France

***Abstract*—**Double gate fully-depleted SOI transistors operating in a remote gate configuration and under closed-loop feedback allow noise performance that exceeds their single gate counterparts by more than an order of magnitude. We leverage this high performance to measure DNA binding in real-time, extracting quantitative association rates that scale with analyte concentration. Our low noise measurements allow a limit of detection (LOD) of ≈ 100 fM by using a sensor chip attached to reusable readout circuitry. Finally, we demonstrate the devices can be operated at high ionic strengths allowing flexibility in assay design for a modest tradeoff in LOD.

I. Introduction

DNA hybridization underlies the detection of numerous infectious diseases and cancers [1]. Measuring the kinetics of DNA binding can provide additional quantitative information. For example, it can enable the detection of mutants, which strongly modulate the association rate with a given probe strand [2]. Numerous types of field-effect transistors (FETs) have been demonstrated to detect DNA binding kinetics. However, to allow detection at femtomolar levels, these have been limited to integrated devices that are single use [3]. Here we show that *n*-channel double gate (DG) fully-depleted silicon-on-insulator (FD-SOI) FETs operating in a closed-loop, remote gate configuration [4] allow low limits of detection (LOD). Furthermore, by separating the sensor that interfaces with the biology from the electronics we obtain a modular platform that allows application-specific customization, by coupling inexpensive sensor chips with reusable circuitry. We first characterize the DG FETs electrically, followed by a characterization of their sensitivity and resolution by using pH measurements. We then measure the real-time binding of DNA on gold surfaces to determine both the association rates and the LOD of our approach. Finally, we explore the effect of ionic strength on both signal amplitude and binding rates.

II. Experimental Approach

A. Double Gate Transistor-based Sensing

The transduction element in our measurements is a DG FD-SOI FET schematically illustrated in Fig. 1A. In this configuration, biomolecular interactions at a working electrode electrically connected to the top-gate generate a voltage V_{TG}. The DG configuration is advantageous for three reasons. First, for a constant I_D the asymmetric gates counteract a small change in V_{TG} by a larger change in V_{BG} resulting in a signal amplification factor (α) [5]–[7]. Second, proportional-integral-derivative (PID) control drastically decreases noise at low frequencies and improves the signal-to-noise ratio (SNR) [4, 5]. Finally, V_{BG} can be adjusted to shift the top-gate threshold voltage V_T to a value optimal for biosensing.

Our FD-SOI transistors were fabricated at CEA-LETI in a process described in [8]. Transmission electron microscope images of a representative device are shown in Fig. 1B while a detailed image of the gate stack is shown in Fig. 1C. Although devices with a wide range of gate lengths, L_G, and widths, W_G, from 10 µm down to deep submicron values are available, we will demonstrate that larger FETs have superior noise performance. The transfer characteristics, I_D–V_{TG}, of an FET with $L_G = W_G = 10$ µm when V_{BG} was stepped between –5 V to 5 V are shown in Fig. 2. The FET exhibits a nearly perfect subthreshold swing of 60 mV/dec at room temperature. At $V_{BG} = 0$ the top-gate threshold voltage, V_T, is ≈ 0.4 V, but this threshold can be reduced to ≈ 0.25 V by applying $V_{BG} \approx 4$ V.

Closed-loop operation of the transistor with PID control is illustrated in Fig. 3 and was described previously [4]–[6]. The voltage from the electrochemical cell is applied to the top-gate, the drain is biased with V_D = 100 mV DC summed with a 10 mV_{pk} AC voltage at frequency F = 100 kHz. The PID controller maintains a constant I_D by adjusting V_{BG} to counteract changes in V_{TG}. An example is shown in Fig. 4, where the PID controller maintains I_D = 0.95 µA when V_{TG} is swept by ±50 mV around V_T = 0.25 V. In response, V_{BG} changes by ≈ ±2 V about a center value of ≈ 4 V. The slope of the curve was used to extract $\alpha = 42.4 \pm 0.7$.

The resolution of our DG FETs was estimated from the noise in V_{BG}. The power spectral density (PSD) of the drain current scaled by I_D (SI_D/I_D) in a FET with L_G = 1 µm, W_G = 10 µm operated in open loop (no PID control) is compared to the same device under PID control in Fig. 5. PID control drastically suppresses noise at low frequencies F < 10 Hz. The corresponding PSD of the back gate voltage, SV_{BG}, is shown in Fig. 6 for DG FETs with different L_G, ranging from 10 µm to 0.1 µm (W_G = 10 µm). Clearly, shorter L_G values increase the integrated noise δV_{BG} (0.1 Hz to 10 Hz), particularly for L_G < 0.5 µm as seen in Fig. 7. Notably, narrow W_G devices, like L_G = 0.2 µm and W_G = 0.24 µm exhibit substantially higher noise. The results clearly show that larger FETs can enable substantial gains in noise performance and thereby precision.

B. Sensor Calibration with pH Measurements

We demonstrate high-resolution pH measurements with DG FETs in closed-loop operation by using the circuit shown in Fig. 3. Time-series measurements with a pH sensor connected remotely to the top gate of the DG FET are shown in Fig. 8A. Phosphate buffered saline (PBS) samples, each adjusted to a different pH value, were measured resulting in a shift in V_{BG}.

2022 International Electron Devices Meeting (IEDM) | 978-1-6654-8959-1/22/$31.00 ©2022 IEEE | DOI: 10.1109/IEDM45625.2022.10019493

Analyzing the time-series data [4], [9] yielded the pH sensitivity from the slope of the curve in Fig. 8B of (1.25±0.02) V per unit of pH, where the uncertainty is the standard error of the fit parameter. The extracted sensitivity is ≈ 20-fold greater than the Nernst potential, $V_N \approx 59$ mV at room temperature.

The time-series data were also analyzed [5] to obtain an average pH resolution of ≈ 5×10^{-4} with expanded uncertainty (k = 2 allowing measurements with 95 % confidence). This pH resolution is ten-fold better than previously reported with solid-state FETs [4], [10] and comparable to ionic-liquid gated devices [5], [6]. Fig. 9 overlays the V_{BG} PSD for each measured pH, showing constant noise levels. These data were used to estimate pH performance [9]. Integrating the PSD over the range of 0.1 Hz to 10 Hz allowed us to estimate back-gate noise $\delta V_{BG} \approx 0.8$ mV. The pH resolution was obtained by scaling δV_{BG} by $\alpha V_N \approx 6\times10^{-4}$, consistent with the time-series analysis.

III. DNA BINDING KINETICS

A. Sample Preparation and Characterization

Fig. 10 shows a schematic diagram of the surface functionalization for DNA measurements. Gold electrodes were first cleaned electrochemically by sweeping a potential between –1.5 V to +1.5 V relative to a pseudo reference electrode at a rate of 0.1 V/s in 50 mM sulfuric acid (H_2SO_4) for a minimum of 10 cycles. Once the reduction peak reached a steady state, the substrates were washed with DI water and incubated in a 10 nM solution containing reduced ssDNA probe (5'-HS-$(CH_2)_6$-TTTCAAGCTGGGTCAGGACA) for one hour at room temperature (immobilization buffer: 1 M $NaHPO_4$, 1× TAE [40 mM Tris, 20 mM acetic acid, 1 mM EDTA], pH = 5). This step was followed by incubation for one hour in 1 mM mercaptohexanol (MCH) in DI water to passivate the unreacted gold. DNA binding measurements were performed by injecting different concentrations of complementary single-stranded DNA diluted in either 150 mM NaCl or 50 mM NaCl and 10 mM $MgCl_2$ in 1× TAE buffer solution (pH = 7.2). The functionalized surfaces were characterized by using electrochemical impedance spectroscopy (EIS) measurements as shown by the Bode plot in Fig. 11. By fitting a simplified Randles circuit equation to the data, we extracted values of the interface resistance of (48.7±0.3) kΩ for the probe surface and (204±2) kΩ upon binding of 10 nM analyte. The uncertainties represent the standard errors in the fit parameters.

B. DNA Binding

DNA binding was monitored by operating a DG FET with L_G = 1 μm and W_G = 10 μm in closed-loop mode (Sec. II A). The functionalized electrodes were connected to the DG FET and the device was operated with V_{TG} = +0.35 V (relative to the working electrode) and a controller set point of I_D = 280 nA. Measurements were performed in 50 mM NaCl. The applied gate bias repelled the probe strands promoting rapid kinetics [11]. After verifying baseline performance, the analyte was introduced and the change in V_{BG} recorded (Fig. 12A). In each case, V_{BG} increased rapidly, offsetting the negative charge accumulating at the top gate due to DNA binding. To quantify the binding rate, we fit the data with a function of the form $V_{BG}(t) = a\left(1 - e^{-(t/\tau)^{0.5}}\right)$, where a is the amplitude at $t = \infty$ and τ is the time constant. For analyte concentrations of 10 nM, 1 nM and 10 pM, τ was (37.3±0.5) s, (44±1) s and (70±2) s respectively. The binding times were consistent with literature values [11] and longer for lower concentrations.

To estimate the LOD of our measurements, we first measured SV_{BG} for each analyte concentration (Fig. 13A). As was the case for the pH measurements, δV_{BG} was invariant with the analyte concentration, averaging ≈ 200 μV. This allowed us to determine the SNR (Fig. 13B), which decreased monotonically with lower analyte concentration. The resulting LOD was ≈ 100 fM at 10 dB. The low LOD is the result of large α and noise suppression at F < 10 Hz due to PID control.

C. Effect of Ionic Strength

We estimated the effect of NaCl concentration on both the signal amplitude and binding kinetics. Higher ionic strengths increase charge screening, whereby the electrostatic potential decays rapidly past the Debye length λ_D. At physiological ionic concentrations (≈ 150 mM NaCl) $\lambda_D \approx 0.7$ nm and the extra charge from hybridized DNA is attenuated. At 50 mM NaCl, λ_D increases to ≈ 1.1 nm. We measured the effect of charge screening on the DNA binding rate for an analyte concentration of 1 nM. The time series data in Fig. 14A allowed the estimation of both the signal magnitude and the binding rate. While the binding rate at both concentrations was comparable as expected (Fig. 14A; *inset*), the magnitude of the measured signal was ≈ 14-fold lower at 150 mM (SNR ≈ 27 dB) than at 50 mM (SNR ≈ 52 dB), see Figs. 15B and 15C. Furthermore, at 150 mM NaCl we can resolve a V_{TG} signal of ≈ 1 mV, assuming α ≈ 42 (Fig. 4), well above the noise floor of ≈ 200 μV.

IV. CONCLUSIONS

We demonstrated measurements of DNA binding kinetics by using high-performance DG FD-SOI devices operated in a remote gate configuration and achieved a low LOD of ≈100 fM. Importantly, our approach separates sensing from electronic transduction, thereby promoting reuse of the readout electronics. It also overcomes a limitation traditionally associated with DG FET devices wherein increased signal amplification did not translate into better noise performance [10]. Finally, the extremely low noise ($\delta V_{BG} \approx 200$ μV) of our approach affords the flexibility to work at physiological ionic concentrations when needed with modest tradeoffs in LOD.

REFERENCES

[1] Sassolas *et al.*, *Chem. Rev.*, vol. 108(1), pp. 109–139, 2008. [2] Xu *et al.*, *Nat. Commun.*, vol. 8(1), p. 14902, 2017. [3] Ziegler *et al.*, *Anal. Chem.*, vol. 93(1), pp. 124–166, 2021. [4] Le *et al.*, *Rev. Sci. Instrum.*, vol. 92(3), p. 030901, 2021. [5] Le *et al.*, *Nanoscale*, vol. 11(33), pp. 15622–15632, 2019. [6] Le *et al.*, *Appl. Phys. Lett.*, vol. 120(26), p. 263701, 2022. [7] Capua *et al.*, in *2021 IEEE International Electron Devices Meeting (IEDM)*, p. 16.2.1-16.2.4. [8] Barraud *et al.*, *Semicond. Sci. Technol.*, vol. 34(7), p. 074001, 2019. [9] Le *et al.*, *Analyst*, vol. 145(8), pp. 2925–2936, 2020. [10] Wu *et al.*, *ACS Nano*, vol. 11(7), pp. 7142–7147, 2017. [11] Rant *et al.*, *PNAS*, vol. 104(44), pp. 17364–17369, 2007.

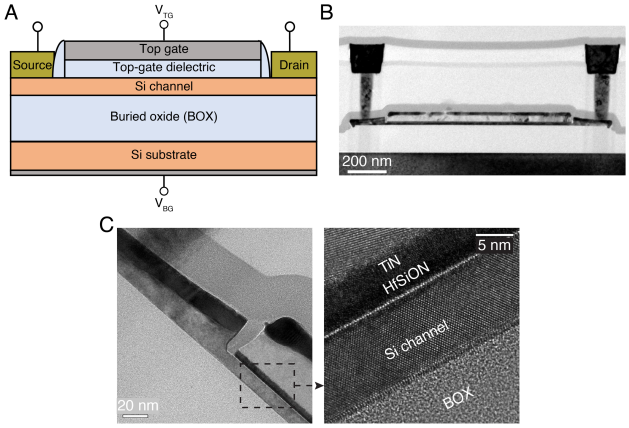

Fig. 1. (A) Device schematic of a double gate FD-SOI field-effect transistor (FET). The top-gate is connected remotely to a sensing surface for biochemical measurements. The device is operated in a DG mode by measuring the large change in the back-gate voltage V_{BG} in response to small voltage changes at the top gate V_{TG}. (B) Transmission electron microscope (TEM) of an FD-SOI FET. (C) TEM image of the FET gate stack.

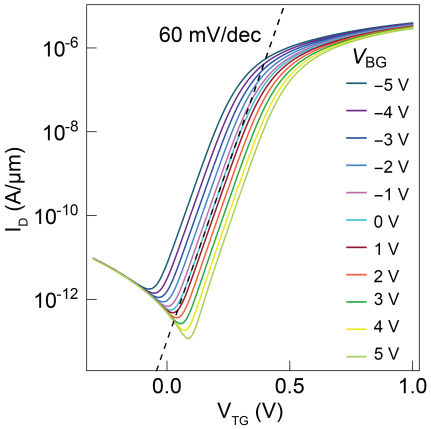

Fig. 2. Transfer I_D– V_{TG} characteristics as a function of back-gate voltage V_{BG} in the –5 V to 5 V range. FET dimensions are $L_G = W_G = 10$ μm.

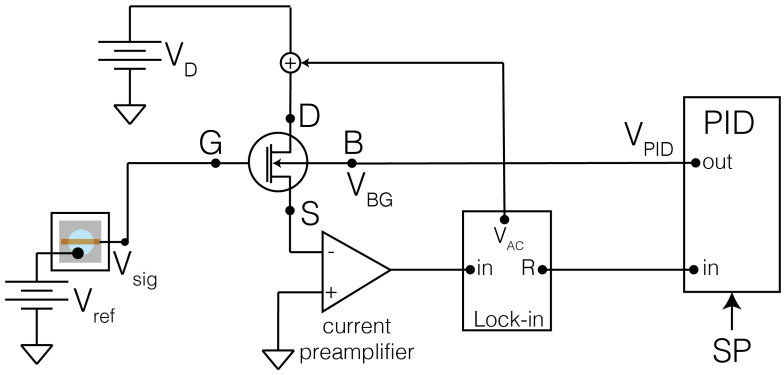

Fig. 3. Schematic of constant-current-mode operation using a proportional-integral-derivative (PID) controller to maintain a constant drain current I_D. Changes in the sensor signal (V_{SIG}) obtained from the electrochemical cell connected to the top gate, G, are nulled by the PID controller by continually changing the back-gate voltage V_{BG}.

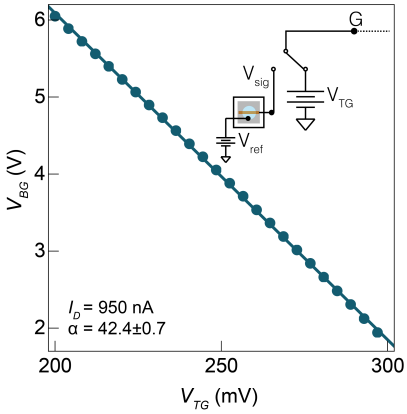

Fig. 4. Amplification of a small V_{TG} signal applied to the top-gate by reading out the back-gate voltage V_{BG} adjusted by the PID controller to maintain a constant I_D = 0.95 μA. The uncertainties (smaller than the symbols) represent one standard deviation. The amplification factor α is obtained from the slope of the line. The uncertainty represents the standard error of the mean of the fit parameter.

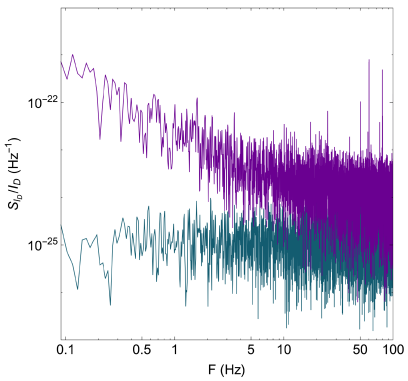

Fig. 5. Power spectral density (PSD) of the current noise for open-loop operation (*purple*) of the FET and for closed-loop operation (*green*). Noise suppression at low frequencies (F < 10 Hz) in the PSD for the closed-loop case directly results in improved measurement resolution.

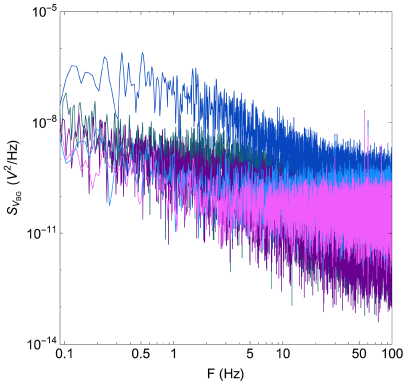

Fig. 6. PSD of the voltage noise of the back gate SV_{BG} in closed-loop mode for L_G = 10 μm (pink) down to 0.1 μm (blue), with 1, 0.4 and 0.2 μm intermediate values. For all devices, W_G = 10 μm. Noise increases as L_G shrinks, especially in the deep submicron regime.

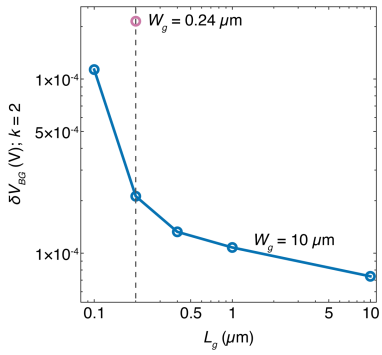

Fig. 7. Noise scaling of the back-gate noise δV_{BG} obtained by integrating the PSD in Fig. 6 from 0.1 Hz to 10 Hz with expanded uncertainty (k = 2) *vs*. FET dimensions. Blue points show dependence on L_G for wide W_G = 10 μm FETs. A nanowire device with L_G = 0.2 μm, W_G = 0.24 μm is shown for comparison. Large devices are beneficial for low noise applications.

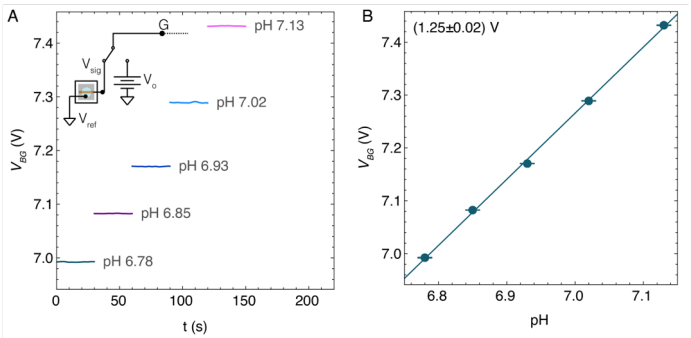

Fig.8. High-resolution pH measurements with double gate FETs in closed-loop mode. (A) Time-series of the back-gate voltage V_{BG} in response to phosphate buffered saline solutions adjusted to different pH values measured with the top-gate. (B) The pH sensitivity was estimated from the data in panel A to be (1.25±0.02) V. The uncertainty in the data represent one standard deviation while that in the sensitivity parameter is the standard error of the fit parameter.

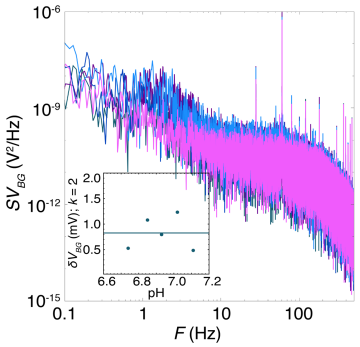

Fig. 9. PSD of the back-gate voltage noise SV_{BG} as a function of pH ranging from 6.8 to 7.1. (inset) The back-gate voltage noise (δV_{BG}) obtained by integrating the PSD from 0.1 Hz to 10 Hz with expanded uncertainty (k = 2) is invariant with changes in pH.

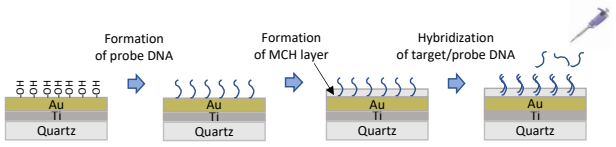

Fig. 10. Surface functionalization and measurement procedure of DNA attached to gold surfaces. Thin film gold electrodes on quartz substrates were cleaned by immersing them in 50 mM H_2SO_4 and sweeping a voltage between −1.5 V and +1.5 V at a rate of ≈ 0.1 V/s. The clean chips were rinsed with deionized water and immersed in a solution containing 10 nM of the probe strand followed by incubation in 1 mM mercaptohexanol (MCH) to passivate the unreacted gold surface. Finally, the analyte strand was injected into solution and the response recorded to measure the kinetics of hybridization.

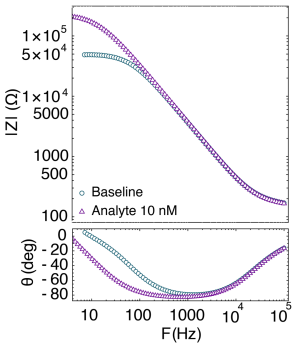

Fig. 11. Electrochemical impedance spectroscopy of the functionalized gold surfaces. Characterization was performed before the addition of analyte (*green*) and upon adding 10 nM of a complementary sequence (*purple*) in 50 mM NaCl with the working electrode held at −0.25 V relative to a pseudo reference electrode and an AC voltage of 10 mV_{pk}.

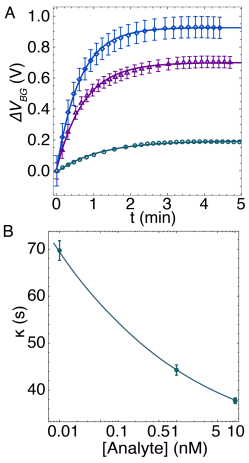

Fig. 12. Kinetics of DNA binding (A) Time-series of DNA binding for 10 nM (*blue*), 1 nM (*purple*) and 10 pM (*green*) analyte concentrations in 50 mM NaCl. Uncertainties represent one standard deviation. (B) Kinetic rate constants as a function of analyte concentration. Uncertainties represent the standard error of the fit parameter.

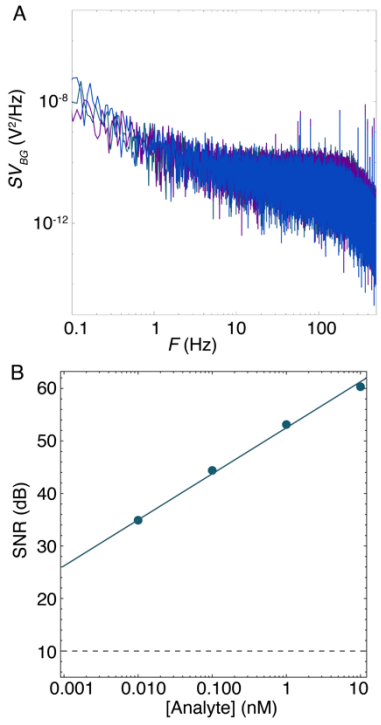

Fig. 13. Scaling of signal with analyte concentration (A) Power spectral density of the back-gate voltage noise (SV_{BG}) overlaid for all analyte concentrations. (B) Signal-to-noise ratio (SNR) of as a function of the analyte concentration. The dashed line at 10 dB represents the noise floor. All measurements were performed with a NaCl concentration of 50 mM.

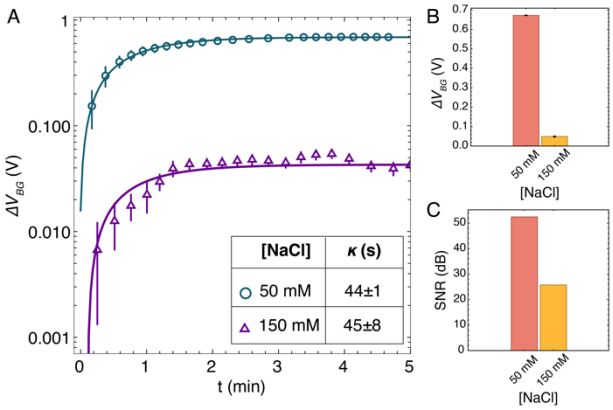

Fig. 14. Effect of electrolyte concentration on DNA binding kinetics and signal amplitude. (A) Time-series of DNA binding with 1 nM analyte and either 150 mM (*purple*) or 50 mM (*green*) NaCl. Uncertainties represent one standard deviation (*inset table*) Kinetic rate constants as a function of electrolyte concentration. The uncertainty represents the standard errors of the fit parameters. (B) Amplitude changes in the back-gate voltage V_{BG} as a function of NaCl concentration measured with 1 nM analyte. Uncertainties represent standard errors of the mean. (C) Signal-to-noise ratio (SNR) as a function of NaCl concentration.